Inorganic Chemistry

Article

pubs.acs.org/IC

Site-Selective High-Resolution X-ray Absorption Spectroscopy and High-Resolution X-ray Emission Spectroscopy of Cobalt Nanoparticles

Timna-Josua Kühn* and Josef Hormes

Institute of Physics, University of Bonn, Nussallee 12, 53115 Bonn, Germany

Canadian Light Source Inc., University of Saskatchewan, 101 Perimeter Road, Saskatoon, S7N0X4, Canada

Nina Matoussevitch

Strem Chemicals GmbH, Berliner Straße 56, 77694 Kehl, Germany

Helmut Bönnemann

Max-Planck-Institut für Kohlenforschung, Kaiser-Wilhelm-Platz 1, 45470 Mülheim a.d. Ruhr, Germany

Pieter Glatzel

European Synchrotron Radiation Facility, Polygone Scientifique Louis Néel, 6 rue Jules Horowitz, 38000 Grenoble, France

Supporting Information

ABSTRACT: The special (macroscopic) properties of nanoparticles are mainly due to their large surface-to-volume ratio. Thus, the separate characterization of geometric and electronic properties of surface and bulk would be favorable for a better understanding of the properties of nanoparticles. Because of the chemical sensitivity of X-ray fluorescence lines, in particular those involving higher lying electronic states, high-resolution fluorescence-detected X-ray absorption spectra (HRFD-XAS) offer these opportunities. In this study, three types of wet-chemically synthesized Co nanoparticles, ∼6 nm in diameter with varying thicknesses of a protective shell, were investigated at the ID26 beamline of the European Synchrotron Radiation Facility. HRFD-XAS spectra at the Co K-edge, that is, X-ray absorption near-edge structure (HRFD-XANES) and extended X-ray absorption fine structure (HRFD-EXAFS) spectra, were recorded via detection of the K$\beta_{1,3}$ fluorescence at specific energies. As these spectra are only partly site-selective due to a strong overlap of the emission lines, a numerical procedure was applied based on a least-squares fitting procedure, realized by singular value decomposition. The detailed analysis of the obtained site-selective spectra, regarding chemical composition and crystallographic phase, using measured and simulated FEFF9-based reference spectra, showed that the metallic core had mainly hexagonal close-packed structure with lattice constants matching bulk Co; the spectra for the shell could be satisfactorily fitted by a mixture of CoO and $CoCO_3$; however, with an obvious need for at least a third compound. To obtain additional information about ligands attached to Co, valence-to-core X-ray emission spectra (VTC-XES) using the K$\beta_{2,5}$ and the satellite structure Kβ'' and VTC-XANES spectra thereof were also recorded, by which the former results are confirmed. Further on, FEFF simulations indicate that a Co−N compound is a very likely candidate for the third component. The presented results clearly show that VTC-XES and HRFD-XAS are suitable tools for the detailed specification of the core and the surface of nanoparticles, in particular upon realizing "real" site-selectivity for XANES and EXAFS with a general strategy applicable to a wide range of systems.

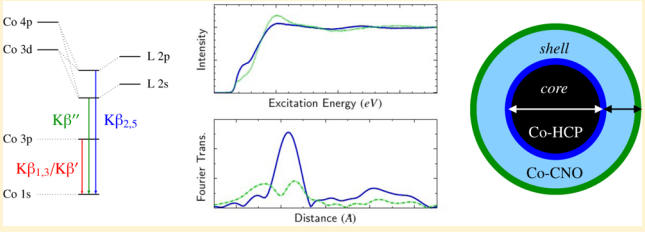

INTRODUCTION

Nowadays, in almost all areas of technology, metallic nanoparticles are of particular interest due to their special thermal, electronic, magnetic, and optical properties. These special properties are mainly due to the nanoparticles' small size, which implies the relevance of quantum effects as well as the significance of the surface: for two nanoparticles 2 nm in size, the surface-to-volume ratio is already 1:1, which by itself implies a huge increase of the total surface for a given amount of nanomaterial, leading to an enhancement of, for example, catalytic effects. "New" properties arise, inter alia, due to surface-to-volume

Received: April 6, 2014
Published: August 8, 2014

   dx.doi.org/10.1021/ic5000183 | Inorg. Chem. 2014, 53, 8367−8375

interactions that are, however, difficult to identify due to the small size that inhibits the application of many "standard" techniques for the characterization of the electronic and geometric properties of nanoparticles. All electron spectroscopic methods, for example, that rely on a specially prepared surface are almost impossible to realize as a surface preparation would strongly modify the complete nanoparticle. Then, the often-occurring lack of long-range order in nanoparticles dramatically complicates diffraction-based methods. X-ray absorption/emission spectroscopy (XAS/XES) is a favorable tool, almost independent of size, degree of crystallinity, and shape/condition of the surface; a determination of geometric as well as electric properties is possible. One drawback emerges, however, as the properties found by (standard) XAS are superposed for the different chemical environments of the chosen element. Thus, no distinction can be made between, for example, the pure metal in a nanoparticle interior and the ligated metal in the outer shells or surface.

Here, high-resolution fluorescence-detected XAS (HRFD-XAS) provides additional opportunities. It is realized by measuring an XAS spectrum via detection of the fluorescence radiation, however, not the "complete" fluorescence but, with the help of a high-resolution XES spectrometer, a certain energy only. Because of the chemical sensitivity of the X-ray fluorescence lines, in particular those involving higher-lying electron states, the emission peak significantly shifts, and HRFD-XAS spectra with strongly different sensitivities toward these distinct chemical environments are gained. This was demonstrated first by M. M. Grush et al. for mixed-valency Mn systems[1] and was successfully reproduced for a Co−CoO compound by our group.[2] M. Haumann et al. also successfully applied this technique to iron.[3,4] P. Glatzel et al. showed for a well-known system[5] that with the help of a numerical procedure, these partially site-selective XAS spectra can be exploited to get "real" site-selective XAS spectra. We extended this numerical procedure to make it applicable to (almost) unknown compounds with differing valencies and successfully tested it on metallic nanoparticles, whose interior (core) and outer shell could be described separately.[6] In that former work, however, the site-selective XANES spectra had not been unique but showed some variance as a result of the still-insufficient resolution.

To improve those former results, similarly synthesized Co nanoparticles were investigated by HRFD-XANES and HRFD-EXAFS, as well as high-resolution nonresonant XES (HR-NRXES), at the ID26 beamline hosted at the European Synchrotron Radiation Facility (ESRF). HR-NRXES at the metal valence band (valence-to-core, VTC) is a well-established technique nowadays, successfully applied to various systems by, for example, P. Glatzel and S. DeBeer.[7−10] It will be demonstrated in this work that with sufficiently high resolution, unique site-selective XAS spectra are achievable, which allow for detailed insight into the electronic and geometric properties of a Co nanoparticle core and shell separately. Furthermore, we will show the value of VTC-XES as it complements the information gained by the first method.

EXPERIMENT

Sample Synthesis. The synthetic methodology for the preparation and anticorrosive stabilization of zerovalent cobalt nanoparticles was recently reviewed in detail by Bönnemann et al.[11] Briefly, air stable Co nanoparticles are obtained by thermolysis of $Co_2(CO)_8$ in the presence of the stabilizing agent $Al(C_2H_5)_3$ (atomic ratio Co/Al = 10:1), with monodispersed size distribution of 6 nm, as determined by transmission electron microscopy (TEM) (see Supporting Information, Figure S1). The single synthesis steps have been: (1) The solid $Co_2(CO)_8$ precursor is given into a toluene bath by addition of the stabilizing agent $Al(C_2H_5)_3$ and is mechanically stirred at room temperature, until all $Co_2(CO)_8$ is dissolved. (2) The mixture is heated to 110 and later to 150 °C and is kept stirring for strictly defined time intervals under toluene reflux, to allow the continuous formation of the Co nanoparticles. (3) After cooling to room temperature, a slow stream of (a defined amount of) diluted oxygen (4.5% O_2 in N_2) is introduced into the suspension of nanoparticles (so-called "smooth oxidation"), with the aim to form a thin protective oxide shell. (4) When the smooth oxidation process is finished, stirring is stopped to allow the nanoparticles to settle down. At last, the supernatant is decanted, and the Co nanoparticles are washed several times with toluene, to get rid of all remnants from the precursor and stabilizing agent.

To avoid possible unwanted oxygen contamination, the whole synthesis is performed under protection gas (pure Ar), and the final nanoparticles are stored in wet form in toluene, until the beginning of the X-ray measurements.

To have Co nanoparticles at hand with different ratios of metallic core to protective shell, step (3) of the synthesis was varied with respect to the speed of the reduced oxygen stream and its total amount. The result was three types of Co nanoparticles that are identically prepared (with respect to the other synthesis steps), but with varying thicknesses of the protective shell.

Noteworthy is that $Al(C_2H_5)_3$ is chosen solely as stabilizing agent/surfactant to have the procedure and the elements involved as simple as possible. The protection from further agglomeration and oxidation is assured by the smooth oxidation (protection gas is utilized nonetheless as a precaution), so that no additional coating is necessary and the number of different metal sites present is minimized.

Synchrotron Beamline. The undulator beamline ID26, at the 6.0 GeVstorage ring of the ESRF, is an insertion device source consisting of three mechanically independent undulators (one 40 mm period and two 35 mm period) that provide a flux of more than 10^{13} photons/with a beam size of 6 mm × 4 mm at the sample. The incident energy is tuned through the Co K-edge by means of a Si(111) cryogenically cooled fixed-exit double-crystal monochromator (DCM). The subsequently emitted Kβ radiation is detected by a high-resolution emission spectrometer that uses four spherically bent Ge(444) analyzer crystals (Ge(111) utilized in fourth order). The instrumental energy resolution of both devices is about 1 eV.

The high-resolution emission spectrometer is described in refs 12 and 13. Briefly (see Figure S2 in the Supporting Information), the incident X-rays, tuned by the DCM, are absorbed by the sample, and the subsequently emitted radiation (partly) reaches the four analyzer crystals. Here it undergoes Bragg diffraction and is focused toward the detector—a single avalanche photo diode—as long as all three components are properly adjusted toward each other and positioned along the Rowland circle of radius R = 0.5 m. The Rowland geometry demands the spherically bent analyzer crystals to have a radius of curvature of 2R, to ensure diffraction with a fixed Bragg angle θ, independently of the diffraction position on the crystal (three positions are shown in Supporting Information, Figure S2).

Thus, it is possible (inter alia) to fix the incident energy and scan the emission energy via the photodiode to perform XES (stepwidth was 0.2 eV), or to tune the incident energy (stepwidth was 0.1 eV) and set the photo diode to one certain emission energy (with uncertainty given by the resolution) to measure HRFD-XAS.

The measurements were performed on cobalt nanoparticles with increasing core-to-shell ratio (from Co-nano-1 to Co-nano-2 to Co-nano-3) as described in the previous section and as references on metallic cobalt foil (Co-foil), cobalt(II)-oxide (CoO), and cobalt(II)−carbonate ($CoCO_3$).

RESULTS

Strategy: Site-Selectivity. On the basis of a previous study of P. Glatzel[5] as well as our recent studies and the present work, a general strategy has been elaborated that allows, in principle, the acquisition of pure site-selective XAS spectra for an arbitrary

dx.doi.org/10.1021/ic5000183 | Inorg. Chem. 2014, 53, 8367−8375

compound with differing valencies (CDV) like the metallic Co nanoparticles with protective shell investigated in this work. As a prerequisite, homovalent references have to be measured that approximately model the different (valence) compounds inherent in the CDV. It is important to note that when focusing on the weaker K$\beta_{2,5}$ emission line (to be precise its satellite Kβ''), instead of K$\beta_{1,3}$, the same strategy allows for ligand-selectivity. That is, it becomes possible to distinguish an element with slightly different electronegativity (due to different ligands) but identical valency.

(1). At first, high-resolution nonresonant X-ray emission spectra (HR-NRXES) of the CDV (the three Co nanoparticle types) and the references must be measured. They are shown in Figure 1. The chemical sensitivity of the K$\beta_{1,3}$

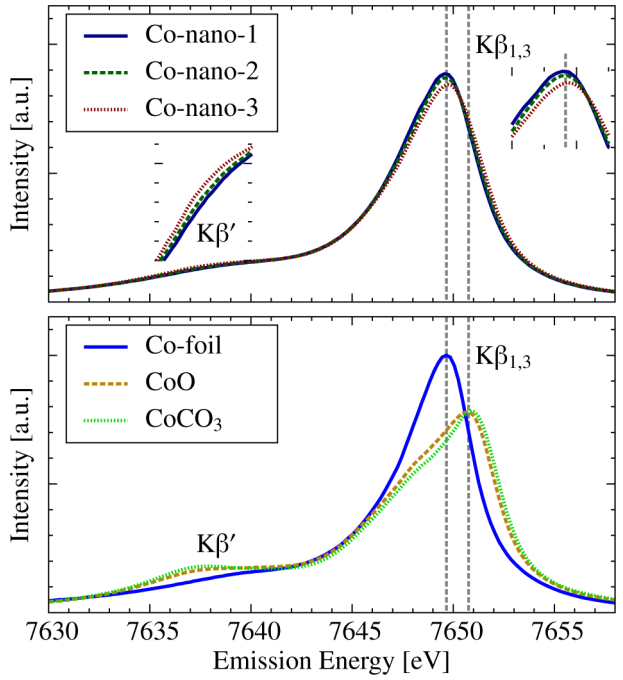

Figure 1. Normalized HR-NRXES K$\beta_{1,3}$ spectra of the three nanoparticles (upper) and the three references (lower). The two vertical dashed lines indicate the peak positions of Co-foil and CoO. For the nanoparticle spectra both peak regions are also shown magnified.

fluorescence (due to the 3p−3d exchange interaction) leads to a significant shift (~1) of the main peak when comparing zerovalent Co-foil and divalent CoO or $CoCO_3$, hence, the necessity of a respective emission energy resolution to exploit this effect. With the help of the reference spectra, the tiny variations visible in the nanoparticles' spectra can be related to an increase of the (mainly) divalent shell fraction as expected from the synthesis. In a second step, the HR-NRXES spectra of the CDV must be fitted by the model references, to find emission energy positions with strongest contrast of the different valence compounds. Such a linear combination fit is shown for Co-nano-3 in Figure 2. The detailed fit results for all three nanoparticle types are given in Table 1. The chosen positions are Pos-2 at 7649.6 eV (K$\beta_{1,3}$ peak of Co-foil) with highest and Pos-3 at 7652.0 eV with lowest Co metal fraction, as well as Pos-1 at 7644.4 with intermediate Co metal fraction. Here it is important that the positions should be chosen symmetrically with respect to

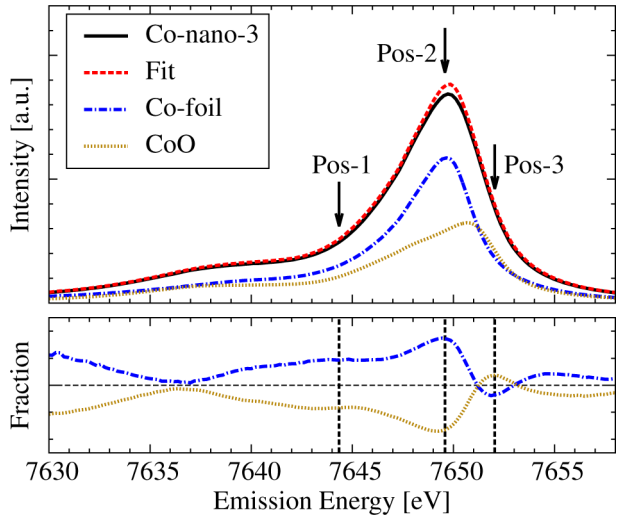

Figure 2. LCF of the K$\beta_{1,3}$ HR-NRXES spectrum of the Co-nano-3 by the references Co and CoO. The lower panel shows the fractions of Co and CoO in Co-nano-3 as determined by the LCF. The three arrows and the vertical dashed lines indicate the positions from which the HRFD-XAS spectra will be extracted.

the main peak and not too far away from it, to avoid strong lifetime broadening distortions (which is not fulfilled for Pos-1; for more details see notes below).

(2). At the positions chosen in step one, HRFD-XAS spectra must be recorded. The XANES as well as Fourier-transformed EXAFS spectra for Co-nano-3 from Pos-2 and Pos-3 are shown in Figure 4. Here the different sensitivities of the Co-nano-3 spectra to the two main valence compounds is visible for XANES (Pos-1 is excluded here; see notes below) in the variations at the edge and whiteline of the spectrum (marked by arrows; compare with Co-foil and CoO in the same figure) and, for EXAFS, in the emerging of the Co−ligand coordination-shell peak (labeled CNO) and decrease of all metal Co−Co coordination-shell peaks (labeled 1 to 4) in the spectrum. The assignments of the coordination-shells are explained in the section Site-Selective EXAFS.

(3). The experimental HRFD-XAS spectra are only partially site-selective due to the strong overlap of the emission lines, albeit the significant shift of the peaks. To get real site-selective spectra, a numerical procedure is required. For this purpose, each HRFD-XAS spectrum S^i_{exp} ($i = 1-6$, for three nanoparticle types and two positions in this case) will be written as a linear combination of the wanted "theoretical" site-specific spectra S_{core} and S_{shell}:

$$S^i_{exp} = c^i_{core} S_{core} + c^i_{shell} S_{shell} \quad (1)$$

with to-be-determined ratio coefficients of $c^i_{core/shell}$. This system of inhomogeneous equations must be solved by a least-squares fit, which will be realized by applying a singular value decomposition (SVD) with the help of the FitIt software.[14] The SVD yields a set of mathematical solutions, that is, functions $S_{core/shell}$ of the excitation energy. These functions are all related to a singular value, which signifies whether it is a necessary "basis function" or just "noise." Thus, the number of necessary fitting components is determined by SVD likewise to Principal Component Analysis (which can be performed by applying a SVD). See refs 14

dx.doi.org/10.1021/ic5000183 | Inorg. Chem. 2014, 53, 8367−8375

Table 1. Results of LCFs of the Co Nanoparticle K$\beta_{1,3}$ HR-NRXES Spectra by the References Co-foil and CoO, as Well as Ratios for Specific Positions Pos-1, 2, and 3.

		overall ratio Co/CoO	*R* factor[a] [× 10^{-5}]	thickness[b] [Å] core/shell	Pos-1	Pos-2	Pos-3
LCF	Co-nano-1	80.5(4): 19.5(4)	64	53.0:3.5	80.3:19.2	87.4:14.9	71.9:28.3
	Co-nano-2	72.6(3): 27.4(3)	32	51.0:4.5	72.5:27.0	80.1:21.3	62.1:38.1
	Co-nano-3	58.5(1): 41.5(1)	8	46.0:7.0	59.3:41.7	67.2:33.7	46.5:53.8
SVD[c]	Co-nano-1		11, 13			98.4:1.6	62.3:37.7
	Co-nano-2		13, 10			74.4:25.6	43.7:56.3
	Co-nano-3		9, 8			69.2:30.8	34.7:65.3

[a]The *R* factor describes the fit quality, and the resulting fit errors are given in brackets (with respect to last digit). [b]The thickness of core/shell is given based on overall ratios, TEM, and a simple geometric model. [c]The results of least-squares fit via SVD, that is, core/shell ratios.

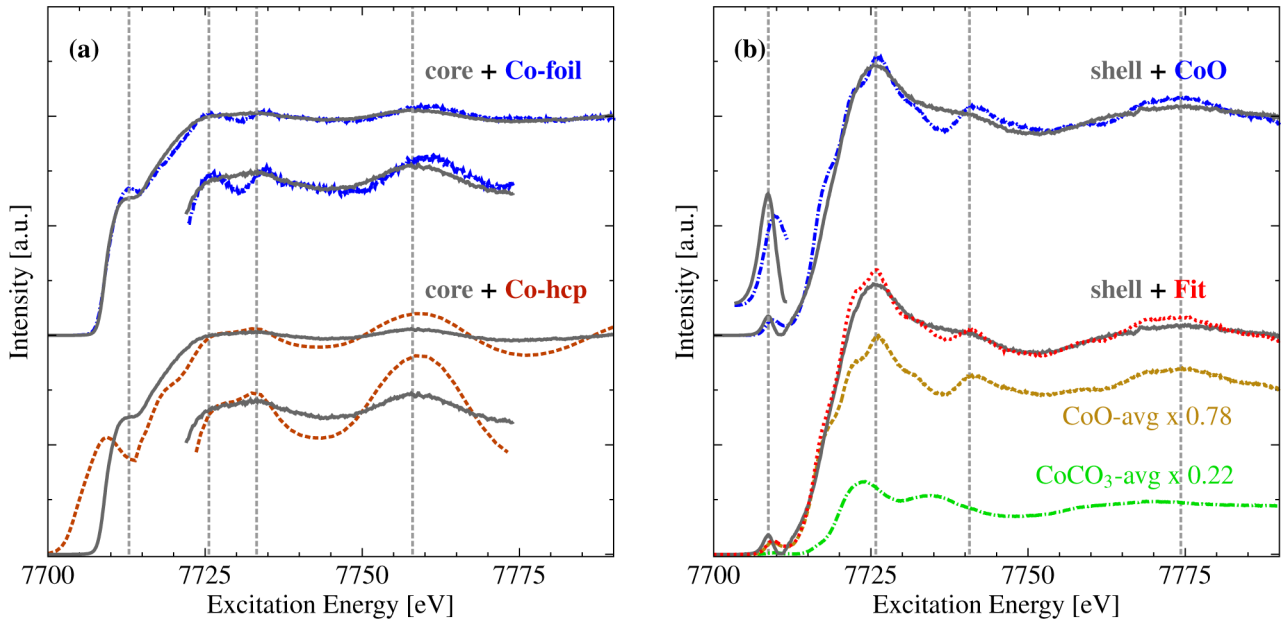

Figure 3. Normalized site-selective Co K-edge HRFD-XANES spectra (a) of the Co nanoparticle core in comparison to Co-foil as well as Co-hcp phase simulated by FEFF and (b) of the Co nanoparticle shell in comparison to CoO as well as a linear combination fit by CoO and $CoCO_3$. The vertical dashed lines mark the significant features of the site-selective spectra.

and 6 for more details. For our nanoparticles the SVD verifies the assumption of two main components ("core" and "shell"). Furthermore, this implies that there is no significant intermediate layer between core and shell as a result of a possible interaction. The functions will be restrained to get unique physical spectra, by demanding (a) the $S_{core/shell}$ to be positive functions of the energy and (b) the corresponding ratio coefficient pairs $c^i_{core/shell}$ to sum up to one. Lastly (c), these coefficients are to be adjusted to those from the linear combination fit (LCF) of the HR-NRXES spectra (step one) upon strict observance of (a) and (b). This is realized by variation of the SVD parameters (see ref 6), which simultaneously alters the (shape of the) theoretical spectra $S_{core/shell}$ and the coefficients $c^i_{core/shell}$, without influencing the fit quality. As can be seen in Table 1, the LCF coefficients are just used as a guideline, which is important to notice, as the LCF is performed with references that are only supposed to be suitable to describe the unknown material under investigation.

Sufficiently high energy resolution of the HRFD-XAS spectra provided, unique site-selective XAS spectra are obtained in the last step. They will be analyzed in the next section.

Notes: As was thoroughly discussed in ref 6, the HRFD-XANES spectra are distorted by the lifetime broadening of the intermediate core-hole (1s in this case), depending on the chosen emission energy position. To correct for this influence all spectra are properly "aligned" instead of performing a three-dimensional deconvolution (remember that HRFD-XAS is just a cut through the three-dimensional excitation energy—emission energy space). This alignment is calibrated via the homovalent reference spectra as, for example, for a metallic Co, the positions of edge, whiteline, and shape resonances must be independent of the emission energy used for recording. As a result all HRFD-XANES spectra from Pos-1 and Pos-3 must be shifted −1 eV and +1 eV, respectively, while those from Pos-2 can be kept unshifted. However, this alignment procedure is only successful if the emission energy positions were chosen symmetrically around a central position. The suitability of this choice can be checked by comparing the average of the HRFD-XANES spectra from the different positions with that from the peak of the model references as shown in the Supporting Information, Figure S3. Pos-1 obviously is not fulfilling these restrictions, hence, its exclusion for XANES. For EXAFS, on the other hand, an "alignment" is implicitly performed via the transformation to *k*-space.

Site-Selective XANES. Actually, it is possible to determine one pair of site-selective spectra for each Co nanoparticle type (1−3); however, since Pos-1 was discarded only two HRFD-XANES spectra are available for each type, which leads to

dx.doi.org/10.1021/ic5000183 | Inorg. Chem. 2014, 53, 8367−8375

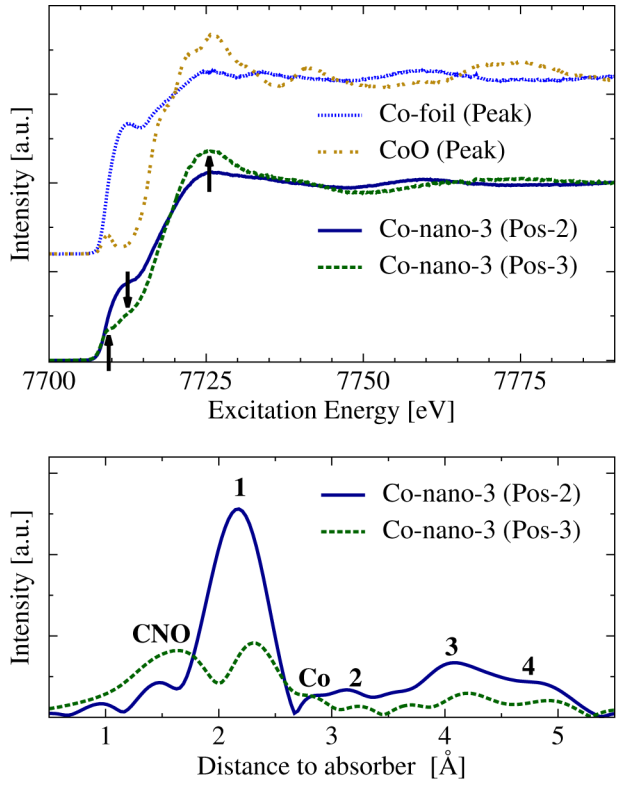

Figure 4. Co K-edge HRFD-XAS spectra of Co-nano-3 from Pos-2 and 3. (upper) Normalized XANES spectra in comparison to references Co-foil and CoO. Change of spectral shapes upon increase of divalent Co is indicated by arrows. (lower) Fourier-transformed k^2-weighted EXAFS spectra. Coordination shells are indicated by labels for Co compound and by numbers for Co metal contributions.

insufficient statistics in the SVD. Consequently, one pair of spectra was determined simultaneously for all three types; the ratios are given in Table 1. These ratios show deviations to those of the K$\beta_{1,3}$LCF to which they have been adjusted, since the references are not matching the real (sought) site-selective compounds in the Co nanoparticles.

The unique site-selective XANES spectra are shown in Figure 3, where they are also compared to their model references Co-foil and CoO. Obviously, neither the nanoparticle core is identical to Co-foil nor the shell to CoO. As XANES spectra are fingerprints of the material, it can be concluded that the core is not (like Co-foil) a 1:1 mixture of Co-face-centered cubic (Co-fcc) and Co-hexagonal close-packed (Co-hcp) (according to FEFF simulations not shown) and that the shell has not exclusively formed a rock salt CoO phase. However, the formal oxidation state can be stated to be +2, identical to CoO. Note that in these interpretations the energetic positions of the shape resonances were the determining factors and not the amplitudes as, in particular for the nanoparticle shell, the Co atoms are incompletely coordinated, which leads to less intense resonances. Besides, more disorder can be expected in the nanoparticles in comparison to the bulk, which further on broadens these resonance features.

As a cross-check, the site-selective XANES spectra are also compared to appropriate HRFD-XANES spectra from Pos-2 and Pos-3 in Figure S5 of the Supporting Information. There the determined site-selective spectra follow the trends that are indicated by the arrows, which denote the increase of the core and shell fraction, respectively.

In the lower part of Figure 3b it becomes obvious that the nanoparticle shell is described much better by both model references CoO and $CoCO_3$ simultaneously. Here a linear combination fit was performed, which resulted in a ratio of 78:22 for CoO/$CoCO_3$. However, the pre-edge position as well as the whiteline structure are not reproduced well with these fit parameters, and consequently, there is a demand for further and/or different components of the shell.

To identify the crystallographic phase of the nanoparticle core as well as further components of the shell, simulations of respective known stable structures were computed via the FEFF9 code.[15] The following settings were used for the XANES simulations: The random-phase-approximation to simulate a screened 1s core-hole; self-consistent potential calculations and the Dirac−Hara plus an imaginary Hedin−Lundquist energy-dependent exchange-correlation potential; and finally, the full-multiple scattering option. The most suitable candidate for the Co nanoparticle core is Co-hcp, shown in the lower part of Figure 3a. However, as can be concluded with the help of the zoom in Figure 3a, to better reproduce the whiteline structure, a further contribution by Co-fcc and/or Co-ε is necessary. These other metal Co phases—Co-ε, Co-fcc, and Co-hcp (again)—are shown in Supporting Information Figure S4. Note that the energy splitting of the (double) whiteline and first shape resonance are properly calculated, however, not the energy position of the edge. Thus, as the Fermi energy is in general not unambiguously calculated by FEFF, the theoretical spectra were aligned to the whiteline/shape resonance.

To further characterize the shell, a hexagonal divalent CoO (wurtzite type) and a Co_3O_4 (spinel structure), which exhibits Co(II)O at the tetrahedral sites and Co(III)O at the octahedral sites, were simulated (not shown). However, none of these compounds were suitable to describe the complete spectral features of the shell spectrum. Nonetheless, wurtzite CoO could have a contribution to the shell, as it exhibits a pre-edge at lower energy compared to rock salt CoO. Moreover, it is noteworthy here that wurtzite CoO is a common phase when dealing with CoO nanoparticles.[16−18]

Site-Selective EXAFS. Analogously to XANES, site-selective EXAFS spectra are obtained via the elaborated strategy. A least-squares fit is performed for all nine HRFD-EXAFS spectra simultaneously, and the resulting core and shell spectra are shown in Figure 5 in comparison to their model references Co-foil and CoO. The amplitudes of the reference spectra are downscaled by a factor of 0.5 to improve comparability. Obviously, the determined core is exclusively metallic since its spectrum is highly similar to that of Co-foil, and no additional peaks due to ligands are visible. However, the ratio of peak 3 to 4 points toward the dominance of the Co-hcp phase and not the Co-fcc phase, demonstrated by FEFF simulations and also shown in Figure 5 (and as was indicated by XANES too). By contrast, the shell spectrum strongly differs from CoO and, moreover, still exhibits the metallic Co−Co first coordination shell labeled 1, which originates in the Co atoms that sit at the inner surface of the nanoparticle shell and are adjoining the metallic Co. On the basis of the dimensions of core/shell that are given in Table 1, one can further estimate the average fraction (for the three types) of inner surface atoms to total shell atoms to about 1/3, which perfectly matches with the amplitude ratio of the shell's and core's peak 1 in Figure 5. However, these atoms are connected only about 50% to Co-metal and 50% to the shell interior (mainly Co−C/N/O); thus, the peak seemingly is too strong by a factor of 2. This will be clarified in an EXAFS fit since all

dx.doi.org/10.1021/ic5000183 | Inorg. Chem. 2014, 53, 8367−8375

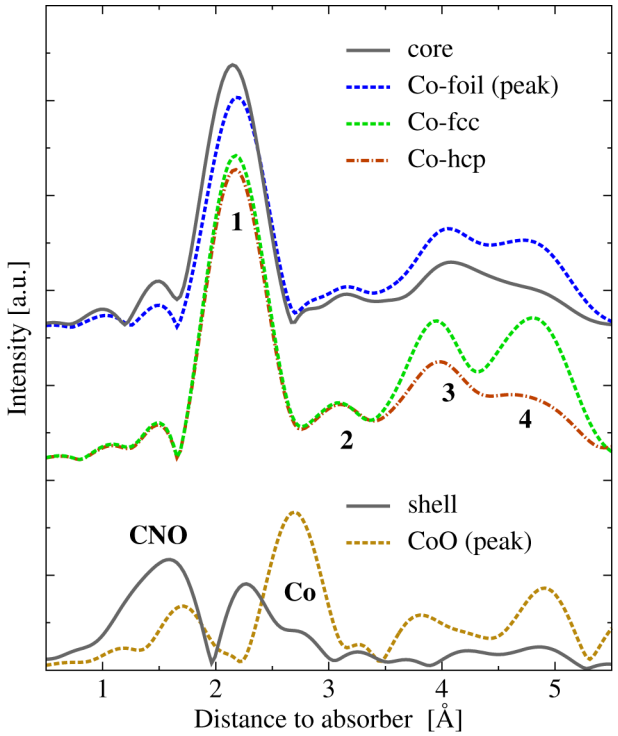

Figure 5. Co K-edge HRFD-EXAFS spectra of the Co nanoparticle core and shell in comparison to respective references (downscaled by 0.5). The core spectrum is further compared to FEFF simulations of Co-fcc and Co-hcp (also downscaled). Labels 1 to 4 refer to metal Co−Co coordination shells; CNO and Co refer to those of a Co compound.

coordination-shell peaks are strongly overlapping (and actually do have a real and an imaginary component).

To identify the site-selective EXAFS spectra, core and shell, they were fitted by FEFF simulations of the single, double, and triple scattering contributions of the Co-hcp phase as well as a Co-CNO compound, which is shown in Figure 6. Here the light elements C, N, and O are treated as one ligand as EXAFS is not capable of distinguishing between scattering atoms with little difference in atomic number.[19] For metallic Co, each of the four coordination shells (labeled 1 to 4) was provided with a Debye−Waller factor (to regard thermal and static disorder), and the lattice constants a and c, an energy shift ΔE_0, and an amplitude-reduction factor δN were set as global fit parameters, resulting in a total of eight parameters versus 20 independent points of the core spectrum within a range from 1 to 5 Å. For the shell spectrum it was only possible to fit a range from 1 to 3 Å, and in addition to the first coordination-shell paths of the Co-hcp phase, the first two single scattering paths of a theoretical Co-CNO compound were used, each with a Debye−Waller factor and a free distance parameter. The detailed results of both fits, as well as analogous simultaneous fits of the HRFD-EXAFS spectra from Pos-2 and 3, respectively, are listed in Table 2.

From these results the Co nanoparticle core can be described as highly crystalline with respect to the local structure, with Co-hcp the dominant phase and lattice constants almost identical to those of a perfect crystal: a = 2.489(6) Å and c = 4.07(2) Å. This is an unexpected outcome as the nanoparticles are really small, only ∼6 nm in diameter. Here it is important to note that a small contribution by Co-fcc is probable, since its paths are identical to those of Co-hcp; just the amplitudes of the third and fourth coordination shells are different. The ratio of the latter two coordination shells restricts this contribution to less than 10%. As the HRFD-EXAFS spectra of the Co nanoparticles from Pos-2 give valuable information about the core too, they were fitted simultaneously (given in Table 2) as well as individually (not shown). From the latter fit, no visible influence of the varying shell thicknesses on the core properties (as accessible by EXAFS) could be identified.

The main results from the EXAFS fits for the Co nanoparticle shell are the development of a local structure with interatomic distances R_{CNO} = 2.00(1) Å for Co−ligand and R_{Co} = 2.99(2) Å for Co−Co and the reduction of the coordination shell number of the metal Co−Co path 1 by δN_{shell} = 0.12(6). This is ∼0.16 of the respective core value of δN_{core} = 0.73(5), which perfectly matches with the considerations at the beginning of this section: 1/3 × 50% ≃ 0.17. Furthermore, no clear structures can be identified above a radial distance of ≃3 Å, which, in accordance with the coordination number reduction, confirms the estimations of the shell thickness based on TEM and the simple geometric model listed in Table 1. As a consequence of this thin shell, no clear crystallographic phase could be found, nor could any Co-compounds be unambiguously assigned.

Valence-to-Core Emission. To shed more light onto the ligands of the Co nanoparticle system, nonresonant high-resolution X-ray emission close to the Fermi level was investigated. This so-called valence-to-core (VTC) XES directly probes the occupied density of states of the materials' valence electrons following off-resonant excitation. In this case, the Co

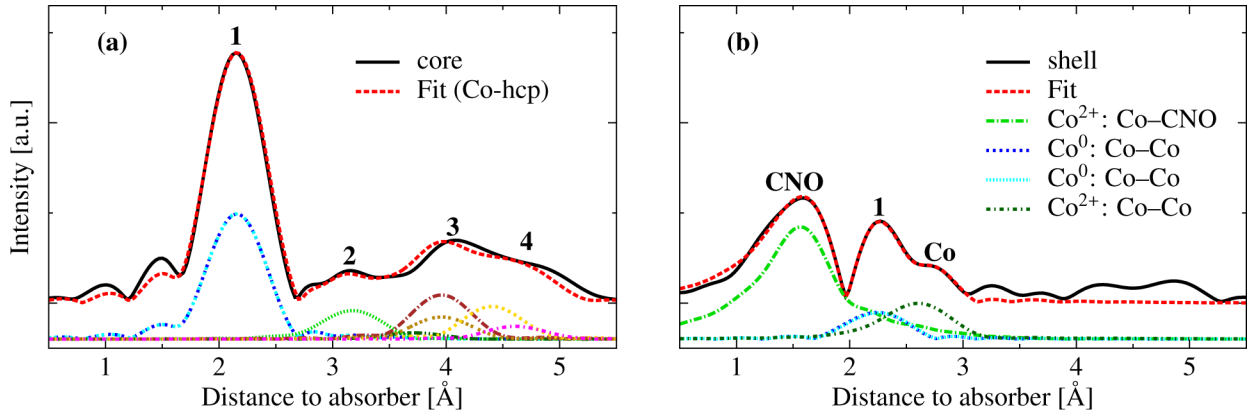

Figure 6. Fits of site-selective EXAFS spectra via FEFF simulations. (a) Core fitted by Co-hcp. (b) Shell fitted by Co-hcp (Co^0) and Co-CNO (Co^{2+}). Also shown are the single-scattering paths for both fits, which reflect the coordination-shells (marked by boldface numbers/labels).

dx.doi.org/10.1021/ic5000183 | Inorg. Chem. 2014, 53, 8367−8375

Table 2. Fits of HRFD-EXAFS Spectra of Co-nano-1, 2, 3 from Pos-2 and 3 (Simultaneously in Each Case) and of the Site-Selective EXAFS Core and Shell Spectrum, Respectively, by FEFF Simulations of Co-hcp and Co-CNO

		perfect crystal	nano-1,2,3 (Pos-2)	core	nano-1,2,3 (Pos-3)	shell
	R factor [$\times 10^{-3}$]		14	8	33	4
Co metal (hcp)	δN	1.00	0.66(4)	0.73(5)	0.22(4)	0.12(6)
	a [Å]	2.507	2.495(04)	2.489(06)		
	c [Å]	4.070	4.070(13)	4.065(18)		
	R_1 [Å]	2.502	2.494(6)	2.489(08)	2.49(1)	2.48(2)
	R_2 [Å]	3.538	3.527(8)	3.520(11)	3.52(1)	
	R_3 [Å]	4.340	4.321(7)	4.311(10)	4.33(2)	
	R_4 [Å]	5.014	4.990(8)	4.978(11)	5.01(2)	
	σ_1^2 [10^{-32}]		5.2(7)	5.6(6)	5(2)	3(4)
	σ_2^2 [10^{-32}]		11(3)	11(2)	10(5)	
	σ_3^2 [10^{-32}]		7(1)	8(1)	6(2)	
	σ_4^2 [10^{-32}]		8(4)	9(4)	2(12)	
Co-CNO	δN_O				0.63(7)	1.1(1)
	R_{CNO} [Å]				2.00(1)	2.00(1)
	R_{CO} [Å]				2.99(2)	2.99(2)
	σ_{CNO}^2 [10^{-32}]				9(2)	10(3)
	σ_{CO}^2 [10^{-32}]				20(5)	18(5)

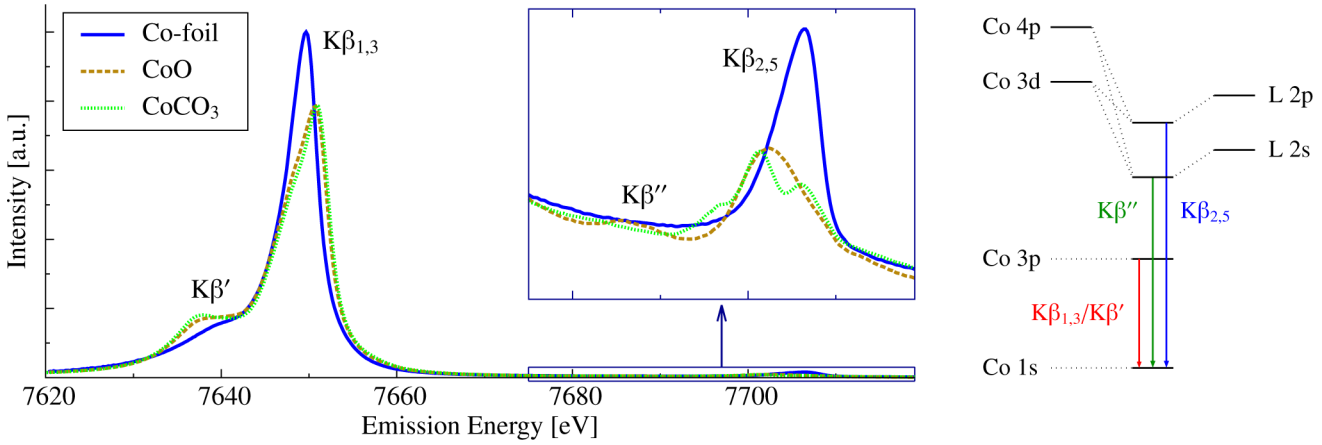

Figure 7. Normalized Kβ emission spectra of the three references Co, CoO, and $CoCO_3$. The main K$\beta_{1,3}$ line and Kβ', as well as the ligand-sensitive K$\beta_{2,5}$ line and crossover resonance Kβ'' are shown. (inset) A zoom to the latter, with ×50 magnification. To the right, transition scheme related to Kβ XES is given.

3d/4p orbitals that are hybridized with the ligand (if first period) 2s/2p orbitals. The HR-NRXES spectra for the references are shown in Figure 7. At lower energies, the K$\beta_{1,3}$ emission line and its low energetic shoulder Kβ' are visible, and at higher energies, the VTC K$\beta_{2,5}$ emission line, which is weaker by about 2 orders of magnitude, is visible. With the help of a magnification by a factor of 50, K$\beta_{2,5}$ and a satellite structure Kβ'' are recognizable. In the right panel of Figure 7, moreover, a scheme of the related electron transitions is given.

To visualize and analyze the nonresonant VTC-XES spectra, the K$\beta_{1,3}$ high-energy tail is subtracted by fitting it with Lorentzian functions. The resulting spectra are given in Figure 8 for all samples and with all significant features—recognizable with the help of the references—labeled and marked. These labels refer to the orbitals related to the electron transitions at the given positions. The assignments are made with the help of FEFF simulations of the angular momentum (l) projected density of states (l-DOS) for the three references Co-foil, CoO, and $CoCO_3$ shown in Figure 9. They are consistent with density functional theory (DFT) calculations on iron compounds.[9] In our simulations, the following crystal phases were used: fcc Co (metal), $fm\bar{3}m$ Co(II)O (rock salt), and $r\bar{3}c$ Co(II)CO_3 (trigonal). Obviously, Co(4p) is describing all significant spectral features alone, however, only as a consequence of its overlap with the ligand 2s/2p orbitals. Thus, the labels in Figure 8 are referring to the ligands. Note that all three references seem to be important to describe the Co nanoparticles.

To get quantitative estimations of the various ligand contributions, an LCF of the Co nanoparticles was performed. It is shown in the Supporting Information, Figure S6 for Co-nano-3, and the complete fit results are given in Table 3. An increased sensitivity of VTC-XES to the different ligands is visible here; however, the absolute ratios are, when compared with K$\beta_{1,3}$ LCF in Table 1, not reflecting the real chemical composition—most probably as a result of the K$\beta_{1,3}$ high-energy tail subtraction. Nonetheless, it can be concluded that the nanoparticle shell is almost equally composed for all three types and that both divalent references CoO and $CoCO_3$ are part of it. However, the fit quality, given by the R factor, is worse by ~1 order of magnitude compared to the K$\beta_{1,3}$ LCF, most visible in the fitting gap from about 7690 to 7698 eV. It indicates the presence of additional Co compounds inherent in the nanoparticle shell, since the Co metal is hardly contributing to this area (see Figure 9a).

dx.doi.org/10.1021/ic5000183 | Inorg. Chem. 2014, 53, 8367−8375

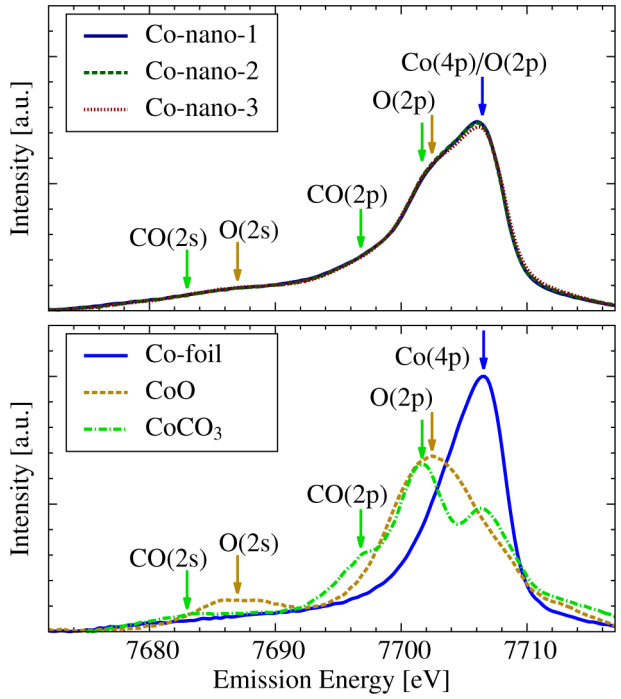

Figure 8. $K\beta_{2,5}$-RXES (or VTC-XES) spectra of the three Co nanoparticle types as well as of the references Co, CoO, and $CoCO_3$. The arrows indicate the significant features of the references, with labels denoting their origin. Here CO denotes contributions by C and O that are inseparable due to strong overlap.

A possible candidate to explain the discrepancies is found by further FEFF simulations of VTC-NRXES spectra of various Co compounds, shown in Figure S7 of the Supporting Information. Since the crossover-peak $K\beta''$ refers to the ligand 2s orbitals of the first period elements, a Co−N compound must give a significant contribution to the aforementioned fitting gap region as it lies in between O(2s) and C(2s). Indeed, the simulations of Co_2N and in particular CoN do confirm this assumption. Here it is important to note that the peaks related to the ligand 2s orbitals show a shift to higher energies with increasing valency, and therefore, as CoN exhibits a valency of +3, a contribution of a Co−N compound with at least this valency is probable. However, it has yet to be shown how and what kind of Co−N compound could form at room temperature (during the "smooth oxidation" process; see section Sample Synthesis). A pathway based on the same precursor we used to get Co nitrosyl at room temperature has been known[20] for a long time; anyway, for nanoparticles there might be "new" possibilities.

XANES from Valence-to-Core Emission. Finally, the low-intensity VTC fluorescence was used to get partly ligand-selective HRFD-XANES spectra of the Co nanoparticles. Since the $K\beta''$ feature nearly is 1 order of magnitude weaker compared to the main $K\beta_{2,5}$ peak, the latter was chosen to record the spectra. To obtain an increased sensitivity to all Co-CNO compounds, the $K\beta_{2,5}$ peak of CoO was selected, and to enhance the metallic Co contribution, the $K\beta_{2,5}$ peak of Co-foil (both peaks were labeled O-2p and Co-4p, respectively, in previous figures) was selected to obtain a similar increase in sensitivity. These two positions are labeled Pos-4 and 5 henceforth, and two selected HRFD-XANES spectra are shown in Figure 10 (the complete spectra are shown in the Supporting Information, Figure S8. The "noise" prior to the edge onset is a remnant of the subtracted elastic peak, which was fitted by Voigt-functions.

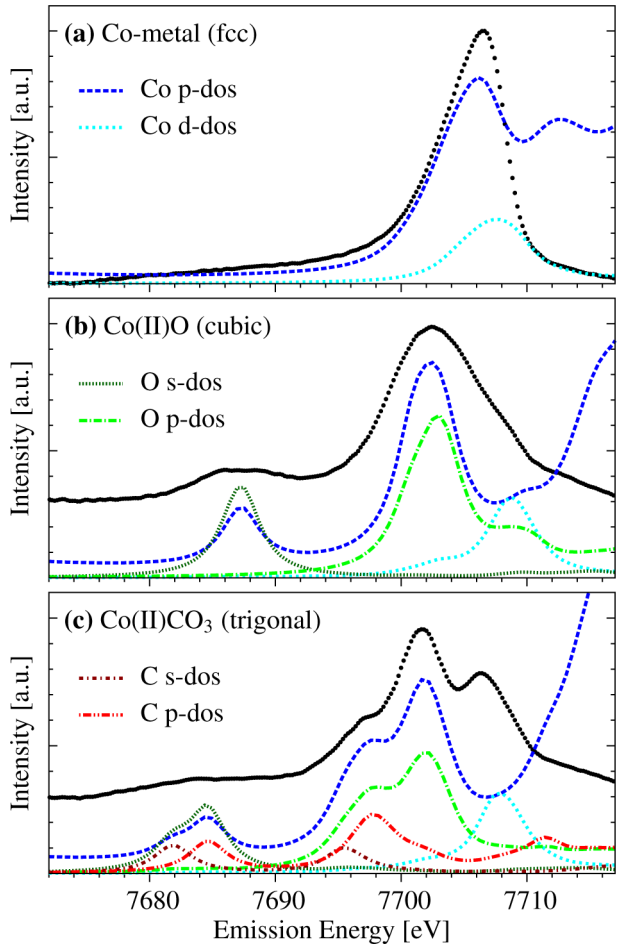

Figure 9. FEFF *l*-DOS simulations in comparison to experimental VTC-XES spectra (black data points •): (a) Co-fcc and Co-foil, (b) rocksalt CoO, (c) $CoCO_3$.

Table 3

$K\beta_{2,5}$ LCF[a]	*R* factor [$\times 10^{-5}$]	ratio (Co/CoO/$CoCO_3$)	
Co-nano-1	555	50.1(4): 37.1(13): 10.7(13)	
Co-nano-2	479	48.9(4): 39.1(12): 10.1(13)	
Co-nano-3	292	48.3(3): 34.4(09): 15.5(10)	
HRFD-XANES LCF[b]		Pos-4	Pos-5
Co-nano-1	36, 35	89.0(4): 11.0(4)	100.0(0): 0.0(0)
Co-nano-2	36, 44	70.0(3): 30.0(3)	85.5(4): 14.5(4)
Co-nano-3	46, 39	66.9(4): 33.1(4)	85.7(4): 14.3(4)

[a]LCF of $K\beta_{2,5}$ HR-NRXES spectra: Co nanoparticles fitted by Co-foil, CoO, and $CoCO_3$. [b]LCF of HRFD-XANES spectra from $K\beta_{2,5}$ fluorescence: The fitting components were the site-specific core and shell spectrum as determined by the least-squares fit. The fit quality is given by the *R* factor, and the fitting errors are given in brackets (with respect to last digit).

Surprisingly, the HRFD-XANES spectrum of Co-nano-1 from Pos-5 almost perfectly resembles the site-selective core spectrum (as determined in the least-squares fit), visible in Figure 10. Motivated by this fact, all six Co nanoparticle spectra are fitted by the site-selective core and shell spectra, with results given in Table 3. Similar to the results from $K\beta_{1,3}$, the Pos-4 spectra show a stronger shell fraction, and the Pos-5 spectra show a stronger core fraction. The fact now that the Pos-5 spectrum of Co-nano-1

dx.doi.org/10.1021/ic5000183 | Inorg. Chem. 2014, 53, 8367−8375

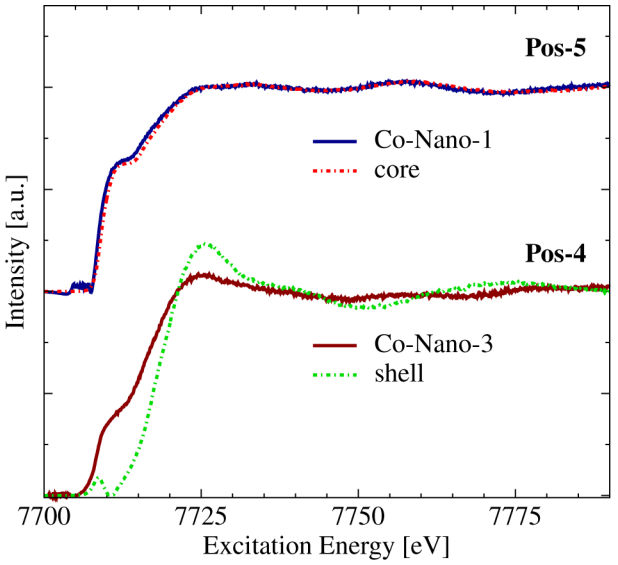

Figure 10. Normalized HRFD-XANES spectrum of Co-nano-1 (recorded at the K$\beta_{2,5}$ peak of Co) compared to the site-selective core (top) and of Co-nano-3 (recorded at the K$\beta_{2,5}$ peak of CoO) compared to the site-selective shell (bottom).

is 100% core actually is similar to the previously found SVD results for the Pos-2 spectrum, where we had a 98:2 ratio in contrast to 87:15 according to the K$\beta_{1,3}$ LCF (see Table 1). Moreover, it is known from DFT calculations[9] that, although the orbitals relevant to K$\beta_{1,3}$ emission are located at the ligands mainly, the major oscillator strength of the transition stems from the metal. Consequently, without further processing, the HRFD-XANES spectrum of the Co nanoparticle core is found here. However, no refinement of the shell composition is possible, upon applying the respective strategy elucidated in the beginning, due to the bad signal-to-noise ratio of the data. For this to be realized, the integration times must be increased significantly, which should also enable recording (partially) ligand-selective HRFD-XAS spectra at the crossover peak Kβ''.

CONCLUSION

The geometric as well as electronic properties of the interior of a Co nanoparticle (its "core") and its surface layers (the "shell") were determined separately for the first time. High-resolution X-ray emission and absorption spectroscopy (HR-XES/HR-XAS) were used to achieve this goal. A numerical procedure, based on singular value decomposition, was applied to get (in contrast to previous studies) *unique* real site-selective HR-XAS spectra that allowed identification of the locally high crystalline hcp phase of the nanoparticles core with lattice constants almost identical to bulk Co and a divalent shell, mainly resembling cubic CoO and trigonal $CoCO_3$, of only about a few monolayers. With the help of nonresonant valence-to-core HR-XES, moreover, the ligands C and O were undoubtedly confirmed, and a Co−N contribution with valency of at least +3 was suggested.

It has become evident that the elaborated strategy for site-selective XAS is advantageous for all types of nanoparticles with weakly and strongly interacting coatings—and for compounds with differing valencies in general—provided there is strong interest in separating bulk and surface layers and that the latter has a significant fraction. Here especially the field of catalysis could benefit from site-selective XAS as well as VTC-XES, as in principle catalytically relevant interconnections inside the surface as well as between surface and bulk can be disentangled. In particular the local atomic arrangement in the surface, provided by site-selective EXAFS, barely is accessible via other techniques.

ASSOCIATED CONTENT

Supporting Information

TEM, drawing of Johann spectrometer, XANES spectra, XES spectra, K-edge spectra. This material is available free of charge via the Internet at http://pubs.acs.org.

AUTHOR INFORMATION

Corresponding Author

*E-mail: kuehn@physik.uni-bonn.de.

Notes

The authors declare no competing financial interest.

ACKNOWLEDGMENTS

The authors wish to thank the European Synchrotron Radiation Facility for beamtime as well as financial support (Experiment No. IH-CH-504) and E. Hallin (Canadian Lightsource) for improving the content and the language of this manuscript.

REFERENCES

(1) Grush, M. M.; Christou, G.; Hämäläinen, K.; Cramer, S. P. *J. Am. Chem. Soc.* **1995**, *117* (21), 5895−5896.
(2) Kühn, T.-J.; Zinoveva, S.; Hormes, J.; Vitova, T.; Louis, R.; Datta, P.; Göttert, J.; Kumar, C. *Adv. Synchrotron Radiat.* **2011**, *0* (2), 1−12.
(3) Leidel, N.; Chernev, P.; Havelius, K.; Ezzaher, S.; Ott, S.; Haumann, M. *J. Inorg. Chem.* **2012**, *51* (8), 4546−4559.
(4) Lambertz, C.; Chernev, P.; Klingan, K.; Leidel, N.; Sigfridsson, K.; Happe, T.; Haumann, M. *Chem. Sci.* **2014**, *5*, 1187−1203.
(5) Glatzel, P.; Jacquamet, L.; Bergmann, U.; de Groot, F. M. F.; Cramer, S. P. *Inorg. Chem.* **2002**, *41* (12), 3121−3127.
(6) Kühn, T.-J.; Caliebe, W.; Matoussevitch, N.; Bönnemann, H.; Hormes, J. *Appl. Organomet. Chem.* **2011**, *25* (8), 577−584.
(7) Swarbrick, J. C.; Kvashnin, Y.; Schulte, K.; Seenivasan, K.; Lamberti, C.; Glatzel, P. *J. Inorg. Chem.* **2010**, *49*, 8323−8332.
(8) Lee, N.; Petrenko, T.; Bergmann, U.; Neese, F.; De-Beer, S. *J. Am. Chem. Soc.* **2010**, *132*, 9715−9727.
(9) Pollock, C. J.; DeBeer, S. *J. Am. Chem. Soc.* **2011**, *133* (14), 5594−5601.
(10) Beckwith, M. A.; Roemelt, M.; Collomb, M.-N.; DuBoc, C.; Weng, T.-C.; Bergmann, U.; Glatzel, P.; deBeer, S. *J. Inorg. Chem.* **2011**, *50* (17), 8397−4097.
(11) Behrens, S.; Bönnemann, H.; Matoussevitch, N.; Kempter, V.; Riehemann, W.; Wiedenmann, A.; Odenbach, S.; Will, S., Eberbeck, D.; Hergt, R.; Müller, R.; Landfester, K.; Schmidt, A.; Schüler, D.; Hempelmann, R. In *Colloidal Magnetic Fluids: Basics, Development and Application of Ferrofluids;* Odenbach, S., Ed.; Springer: Berlin, Heidelberg, 2009; pp 1−69.
(12) Glatzel, P.; Sikora, M.; Fernández-García, M. *Eur. Phys. J.: Spec. Top.* **2009**, *169*, 207−214.
(13) Glatzel, P.; Sikora, M.; Smolentsev, G.; Fernández-García, M. *Catal. Today* **2009**, *145*, 294−299.
(14) Smolentsev, G.; Guilera, G.; Tromp, M.; Pascarelli, S.; Soldatov, A. V. *J. Chem. Phys.* **2009**, *130* (17), 174508.
(15) Rehr, J. J.; Kas, J. J.; Prange, M. P.; Sorini, A. P.; Takimoto, Y.; Vila, F. *C. R. Phys.* **2008**, *10* (6), 548−559.
(16) Yin, J. S.; Wang, Z. L. *Phys. Rev. Lett.* **1997**, *79* (13), 2570−2573.
(17) Seo, W. S.; Shim, J. H.; Oh, S. J.; Lee, E. K.; Hur, N. H.; Park, J. T. *J. Am. Chem. Soc.* **2005**, *127*, 6188−6189.
(18) Nam, K. M.; Shim, J. H.; Han, D.-W.; Kwon, H. S.; Kang, Y.-M.; Li, Y.; Song, H.; Seo, W. S.; Park, J. T. *Chem. Mater.* **2010**, *22* (15), 4446−4454.
(19) Rehr, J. J.; Albers, R. C. *Rev. Mod. Phys.* **2000**, *72*, 621.
(20) Strouse, C. E.; Swanson, B. I. *J. Chem. Soc. D* **1971**, *117*, 55−56.